Steel and Composite Structures, *Vol. 25, No. 5 (2017) 545-556*
DOI: https://doi.org/10.12989/scs.2017.25.5.545

Axial load behavior and stability strength of circular tubed steel reinforced concrete (SRC) columns

Biao Yan[1], Jiepeng Liu[*2] and Xuhong Zhou[2]

[1]*Department of Engineering Mechanics, School of Civil Engineering and Mechanics, Lanzhou University, No.222, Tianshui Road(south), Chengguan Dstrict, Lanzhou 730000, China*
[2]*Department of Civil Engineering, School of Civil Engineering, Chongqing University, No.174, Shazheng Street, Shapingba District, Chongqing 400044, China*

(*Received February 24, 2017, Revised July 16, 2017, Accepted September 14, 2017*)

Abstract. The tubed steel reinforced concrete (SRC) column is a composite column in which the outer steel tube is mainly used to provide confinement on the core concrete. This paper presents experimental and analytical studies on the behavior of circular tubed SRC (TSRC) columns subjected to axial compression. Eight circular TSRC columns were tested to investigate the effects of length-to-diameter ratio (*L/D*) of the specimens, diameter-to-thickness ratio (*D/t*) of the steel tubes, and use of stud shear connectors on the steel sections. Elastic-plastic analysis on the steel tubes was used to investigate the mechanism of confinement on the core concrete. The test results indicated that the tube confinement increased the strength and deformation capacity for both short and slender columns, and the effects on strength were more pronounced for short columns. A nonlinear finite element (FE) model was developed using ABAQUS, in which the nonlinear material behavior and initial geometric imperfection were included. Good agreement was achieved between the predicted results using the FE model and the test results. The test and FE results were compared with the predicted strengths calculated by Eurocode 4 and the AISC Standard. Based on the analytical results, a new design method for this composite column was proposed.

Keywords: circular TSRC; axial compression; stability strength; finite element analysis; column curve; design method

1. Introduction

SRC column consists of structural steel sections, reinforcing bars and concrete. Such a structural form combines the advantages of both steel and concrete, and thus the columns show high load-bearing capacity, inherent ductility, fire resistance, and large energy absorption capacity (El-Tawil and Deierlein 1999, Choi *et al.* 2012, Ky *et al.* 2015). Due to the flexible arrangement of the steel sections, SRC can also be used as special-shaped column or boundary element of shear wall (Chen *et al.* 2016, Massone *et al.* 2017). However, the construction process of the reinforcing bars and the steel sections in the beam-column connection is complex (Wang *et al.* 2015, Chang *et al.* 2016), and the reinforcement cage further adds difficulty in concrete casting (Fig. 1(a)). To reduce the complexity, a new type of composite column which named tubed SRC column (TSRC), was proposed by Zhou and Liu (2010).

The TSRC column is a composite column in which the outer steel tube is mainly used to provide confinement to the core concrete. Compared with SRC column, the reinforcement cage in SRC column is replaced by the outer thin-walled steel tube in TSRC column. To maximize the tube confinement on concrete and reduce the possibility of tube buckling, the outer thin-walled steel tube was chosen to have a gap at the end of the column. A TSRC beam-column connection is shown in Fig. 1(b). As the improvement of SRC column, the tube of TSRC column can offer effective confinement on the concrete core and prevent the concrete cover from spalling off. The quality of concrete casting can also be improved since no reinforcement cage is required.

The tubed plain concrete column was first studied as a means of loading concrete filled steel tube (CFST) columns by Gardner and Jacobson (1967). Tomii *et al.* (1985) first investigated the behavior of tubed RC (TRC) short columns. The research aimed to prevent the RC short columns from undergoing brittle shear failure, and the test results indicated that the energy absorption capacity of the TRC short columns improved due to further confinement of outer steel tubes. Up to now, extensive studies on TRC columns have been performed with promising results. However, as a new type of composite columns, the research on TSRC columns is very limited. Compared to SRC columns, the TSRC short columns exhibit higher strength, plastic deformation capacity, and energy dissipating capacity while under the same volumetric steel ratio and axial compressive load (Gan *et al.* 2011). Experimental and analytical studies on the behavior of square TSRC columns subjected to eccentric compression was conducted by Wang *et al.* (2016), the test results indicated that the encased steel sections worked with the concrete compatibly due to the confinement from the steel tube, and a simplified method to estimate the capacity interaction diagram of square TSRC column was proposed.

*Corresponding author, Professor,
E-mail: liujp@cqu.edu.cn

Copyright © 2017 Techno-Press, Ltd.

ISSN: 1229-9367 (Print), 1598-6233 (Online)

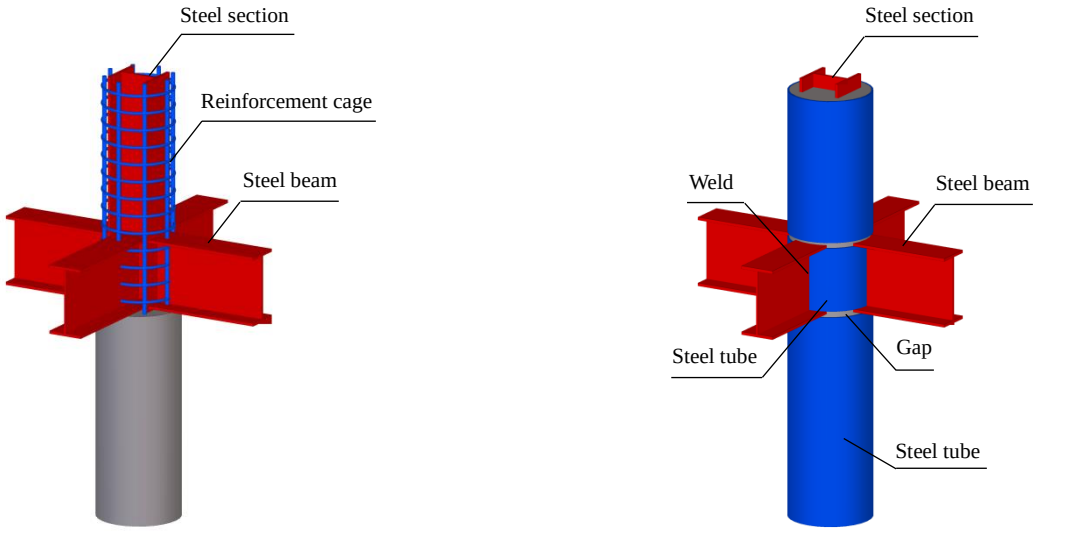

(a) SRC column-beam connection (b) Tubed SRC column-beam connection

Fig. 1 SRC and tubed SRC column-beam connections in structural frames

Previous studies have focused on the behavior of TSRC short columns. The performance of this new composite column with large slenderness ratio is also noteworthy of concern since the high load-bearing capacity of the column may lead to relatively smaller cross-section. For this purpose, an experimental investigation of circular TSRC columns with different slenderness ratios under axial compression is conducted. ABAQUS is used to perform the FE analysis. The feasibility using design codes, such as Eurocode 4 (CEN 2004) and AISC 360-16 (AISC 2016), to predict the value of the reduction factor for the relative slenderness $\bar{\lambda}$ is also addressed, in which some necessary modifications need to be made.

2. Experimental program

2.1 General

As presented by Liu *et al.* (2015), axial and eccentric compression behavior of 12 circular TSRC short columns has been investigated. As a series of tests, axial load behavior of slender columns were also conducted by the authors, and the remaining tests will be given in this paper. In order to investigate the stability strength of circular TSRC columns, further tests include columns with L/D of 6, were performed under axial compression, where the specimen details are provided in Table 1. For convenience of the following explanation, the specimens were renamed in this paper, as shown in Table 1. Fig. 2 shows the details of the test columns. The steel tube terminated 100 mm away from the ends of the column, and the gap was chosen to have a height of 10 mm. A 10 mm thick steel end plate was welded to the ends of specimens. To prevent local failure at the ends, stiffeners were disposed near the ends (see Fig. 2(a)).

The stiffeners were chosen as 20 mm high and 5 mm thick. As can be seen from Fig. 2(c), the ends of the steel section were also strengthened by welding stiffeners. Before pouring concrete, the steel section was arranged at the appropriate position by welding short bars on the ends of the steel section, and the ends of the steel section were pasted on the end plate only by gravity (no welding seam) since the column would only suffer axial load.

Details of the test variables for each specimen are provided in Table 1. The nomenclature of the specimens in the table can be explained by the example of specimen C-200-6-S: C denotes circular TSRC column; 200 represents the diameter of the specimen in millimeters; 6 represents the length-to-diameter ratio; S denotes studs, and omitting this letter represents that studs were not used (see Fig. 2(c)). Parameters for the tests include the following: length-to-diameter ratio (L/D = 3, 6), tube diameter-to-thickness ratio (D/t = 120, 133), and stud shear connectors (used or not used).

A cold-formed steel plate was used to fabricate the outer circular tube, and the welding seam was strengthened by an additional plate with 50 mm width to prevent local tension fracture. The encased steel section was a hot-rolled *H* section. To determine the material properties, along the rolling direction and the perpendicular direction of the tube, two groups of 6 tensile coupons were tested; and along the longitudinal direction of the *H* section, one group of 3 tensile coupons was tested. The average yield strengths are presented in Table 1, where f_{yt} is the yield strength of the tube, and f_{ys} is the yield strength of the steel section. The cubic strength of concrete (f_{cu}) at the time of the tests is determined by 150 mm cubes, and the axial compressive strength of concrete (f_{co}) is determined by prisms with dimensions of 150 mm×150 mm×300 mm. E_t, E_s, and E_c are the elastic modulus of the steel tube, steel section, and concrete, respectively.

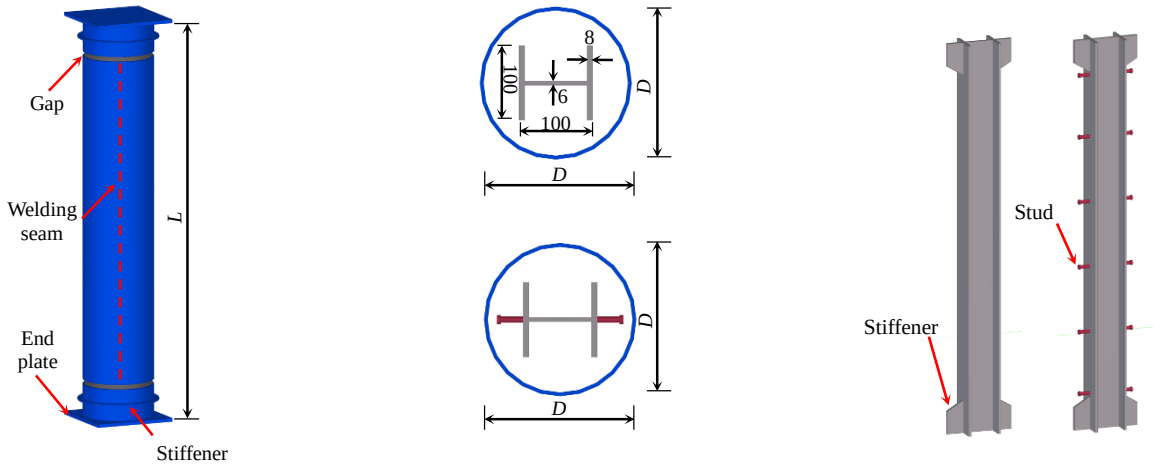

(a) Test specimen (b) Cross-sections (c) Steel sections

Fig. 2 Details of the test columns

Table 1 Properties and results of the specimens

Specimen	L (mm)	D (mm)	t (mm)	D/t	Studs	f_{yt} (MPa)	f_{ys} (MPa)	f_{cu} (MPa)	f_{co} (MPa)	E_t (GPa)	E_s (GPa)	E_c (MPa)	N_{ue}/kN	Global imperfection	Boundary condition
C-200-3	600	200	1.5	133	/	324.4	285.4	80.6	61.1	203	205	36483	3421	/	Fixed
C-200-3-S	600	200	1.5	133	@100	324.4	285.4	80.6	61.1	203	205	36483	3423	/	Fixed
C-200-6	1200	200	1.5	133	/	324.4	285.4	80.6	61.1	203	205	36483	2851	2.6 mm	Pin-ended
C-200-6-S	1200	200	1.5	133	@200	324.4	285.4	80.6	61.1	203	205	36483	2933	1.8 mm	Pin-ended
C-240-3	720	240	2.0	120	/	290.1	285.4	80.6	61.1	199	205	36483	4408	/	Fixed
C-240-3-S	720	240	2.0	120	@100	290.1	285.4	80.6	61.1	199	205	36483	4400	/	Fixed
C-240-6	1440	240	2.0	120	/	290.1	285.4	80.6	61.1	199	205	36483	3797	3.0 mm	Pin-ended
C-240-6-S	1440	240	2.0	120	@200	290.1	285.4	80.6	61.1	199	205	36483	3439	5.6 mm	Pin-ended

2.2 Test set-up and instrumentation layout

The tests were performed suing the 5000kN hydraulic compression machine, as shown in Fig. 3. For short columns (L/D=3), the articulated rigid plates of the press machine were employed to simulate the fixed boundary conditions. A load sensor was used to measure the axial load and correct the measured value of the compression machine. For slender columns (L/D=6), V-shape edges were used to ensure single-curvature bending behavior. Two 50 mm thick plates were fixed between each V-shape edges and the ends of the specimen prior to loading, and the axial load was measured by the corrected compression machine. Fig. 3 depicts the instrumentation layout for the specimens. Four linear voltage displacement transducers (LVDTs) were used to monitor the axial shortening at the ends of the specimens. For slender columns, five additional LVDTs were used along the specimen span to monitor the deflections. Eight strain gauges were glued onto the tube to measure the axial and transverse strains at the mid-height of the columns, as shown in Fig. 3. A computerized data-acquisition system was used to collect the load, deformation, and strain data. Load intervals of less than one-tenth of the estimated capacity were used. Each load interval was maintained for approximately 2 mins. To investigate the softening response of specimens, the load was slowly and continuously applied near and after the peak load.

3. Experimental results and discussions

3.1 Failure mode and load-deformation relationship

Fig. 4 illustrates the failure modes of short specimens. Similar shear failure was observed by splitting the steel tube from the concrete. The load (N) versus axial displacement (Δ) curves are presented in Fig. 5. The steel tubes yielded when the applied compression almost reached the ultimate value. Compared to the specimens without studs, the shear-sliding angle of those with studs decreased since the studs

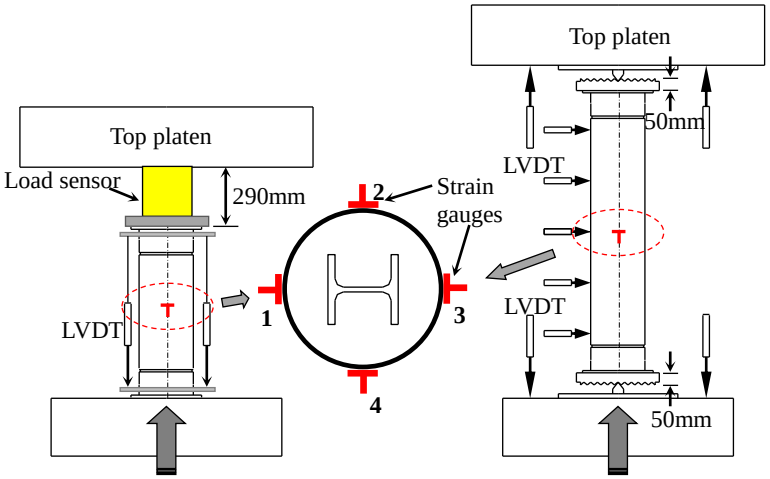

(a) Short column (L/D=3) (b) Slender column (L/D=6)

Fig. 3 Schematic view of test set-up and instrumentation layout

(a) C-200-3 (b) C-200-3-S

Fig. 4 Failure modes of short columns (L/D = 3)

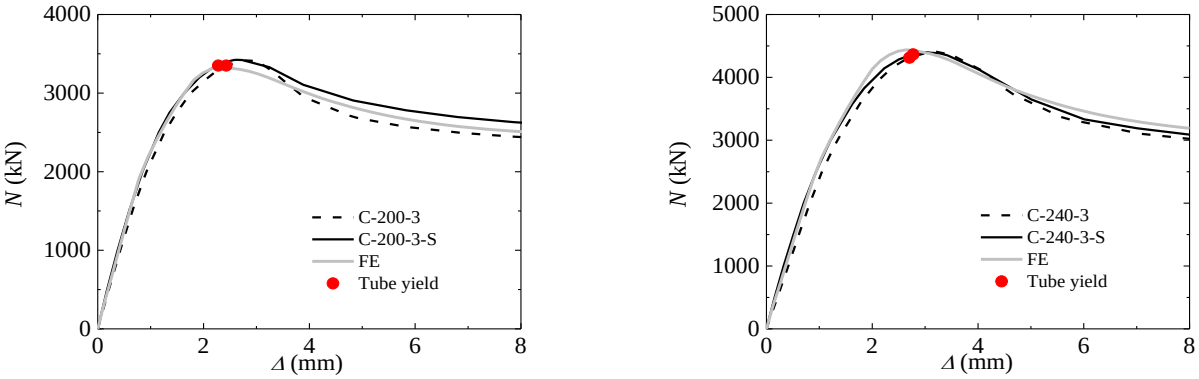

Fig. 5 Load (N) versus axial displacement (Δ) curves of short columns

(a) C-200-6 (b) C-200-6-S

Fig. 6 Failure modes of slender columns (L/D = 6)

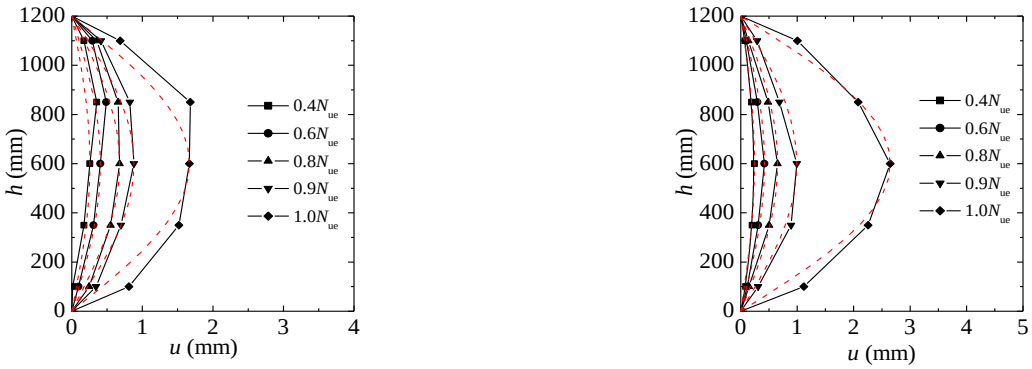

(a) C-200-6 (b) C-200-6-S

Fig. 7 Lateral deflection along slender columns at different load levels

constrained the shear-sliding deformation of concrete. However, the stud shear connectors have no influence on the load-bearing capacity of short circular TSRC columns since the capacity of the specimen with studs is almost the same as that of the specimen without studs.

A comparison of the failure modes of the slender specimens was conducted, as shown in Fig. 6. Two typical specimens were selected to describe the lateral deflection development, as shown in Fig. 7. Obvious lateral deflection was observed during the tests, and the deflection curves were approximately in the shape of half-sine wave. Fig. 8 presents the axial load (N) versus mid-height lateral deflection (u_m) curves of slender specimens. Curves of axial load (N) versus axial shortening displacement (Δ) were not selected since the accuracy of measurement was greatly affected by the interstices between V-shape edges, thick plates, and the ends of specimen. Local buckling occurred near the mid-height of the specimens at the postpeak stage.

Little surprise, the ultimate strength of specimen C-200-6-S is less than that of specimen C-200-6 due to the larger imperfection (see Table 1). Concrete crushing was found at the location where tube buckling occurred. The failure of slender specimens arose from stability during the tests, so the studs had no significant influence on the failure mode, strength, and ductility. The equations recommended in ACI 318-14 (ACI 2014) and Eurocode4 (CEN 2004) were applied to calculate the limits of diameter-to-thickness ratio. According to the codes, the limits of the specimens with diameter of 200mm (D/t = 133) are 70.2, 108.8, respectively. However, these codes were developed for CFST columns. For circular TSRC columns, local buckling occurred at the postpeak stage, the codes are conservative since no axial load was directly applied on the steel tube.

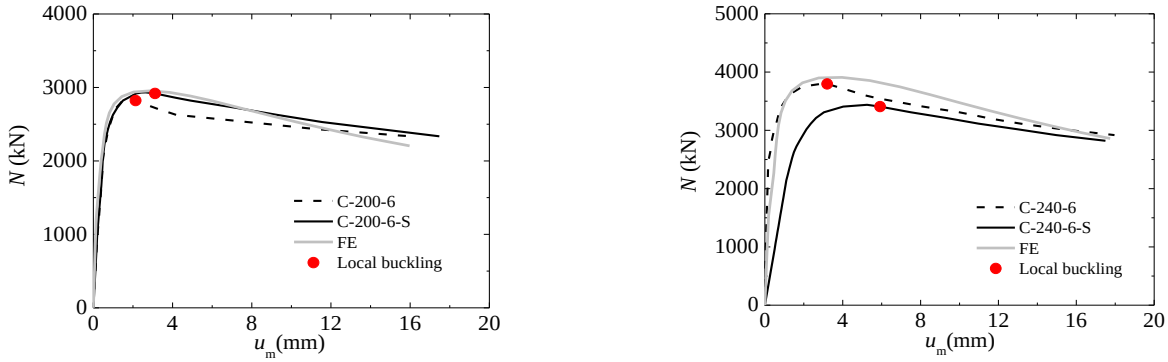

Fig. 8 Axial load (N) versus mid-span lateral deflection (u_m) curves of slender columns

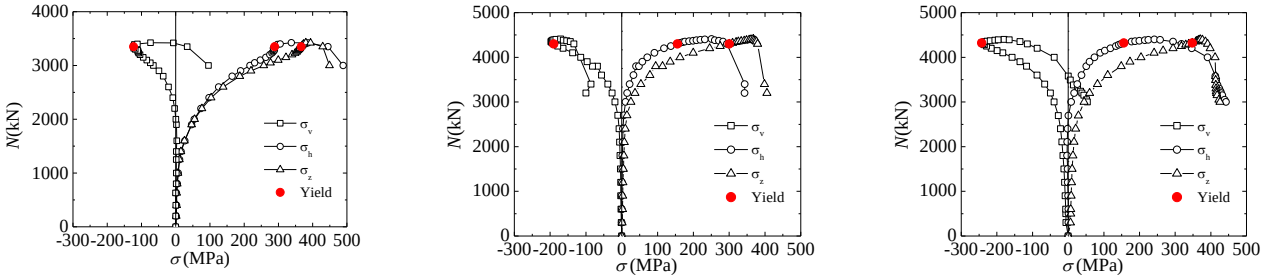

(a) C-200-3-S (b) C-240-3 (c) C-240-3-S

Fig. 9 Load-tube stress responses of short columns

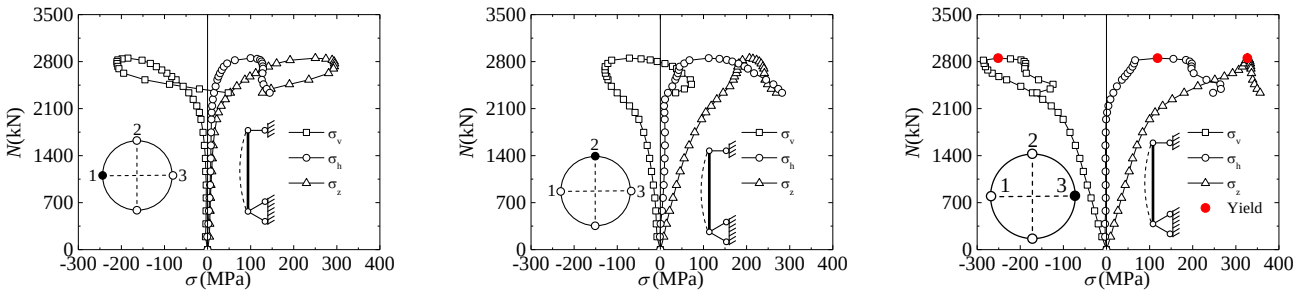

(a) Gauging point 1 (b) Gauging point 2 (c) Gauging point 3

Fig. 10 Load-tube stress responses of C-200-6

3.2 Failure mode and load-deformation relationship

The elastic-plastic analysis method was used to analyze the stress state of steel tubes based on the measured strains. Fig. 9 illustrates the analysis results of short columns, in which σ_v and σ_h are the longitudinal stress and the hoop stress of steel tube, respectively; σ_z is the equivalent stress determined by the following equation

$$\sigma_z = \frac{\sqrt{2}}{2}\sqrt{\left(\sigma_v - \sigma_h\right)^2 + \sigma_v^2 + \sigma_h^2} \quad (1)$$

The load-tube stress responses of the short columns are presented in Fig. 9. The average stress was chosen in the figure since the stress along the tube circumference was uniform. The steel tube yielded when the applied compression was close to the ultimate strength. The stresses increased rapidly when the load attained approximately 65% of the ultimate strength due to the plastic expansion of concrete. When the applied load achieved the peak value, the steel tube was mainly in tension since the longitudinal stress was much lower compared to the hoop stress, which resulted in a high level of confinement of the concrete.

The load-tube stress responses of the slender columns are presented in Fig. 10. The locations of gauging points 1, 2, 3, and 4 are shown in Fig. 3. The loading states of the tubes at the four points were different since failure of the slender specimens arose from instability. Therefore, the results of the gauging points must be discussed respectively.

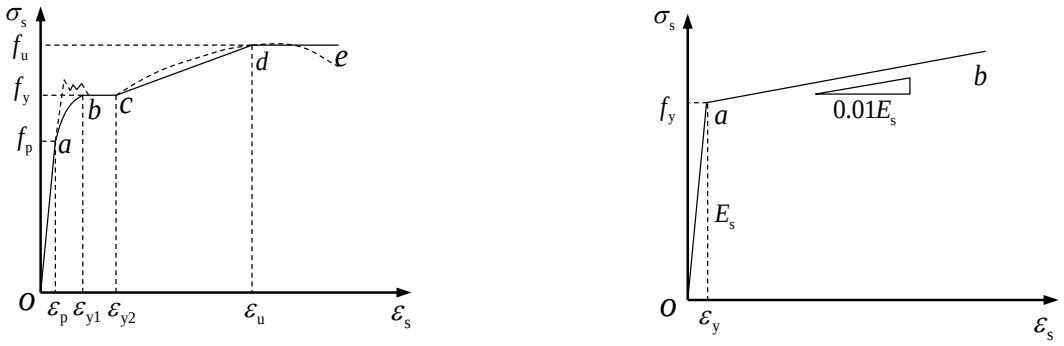

(a) Mild steel (b) High strength steel

Fig. 11 Stress-strain relation for steel

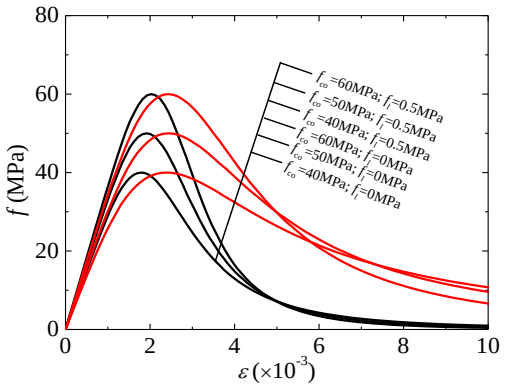

Fig. 12 Equivalent stress-strain curves of concrete ad -opted by finite element model

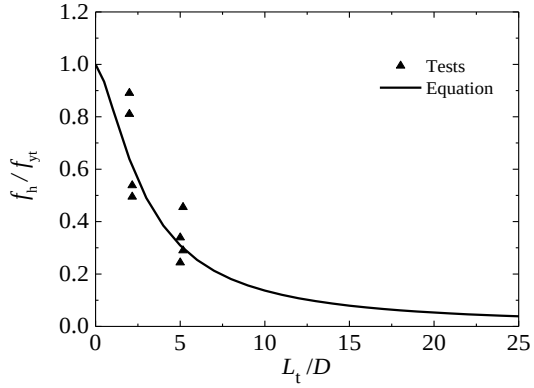

Fig. 13 Effect of length-to-diameter ratio on the average hoop stress

The tendency of the deflection is also shown in this figure. As can be seen, the stresses of gauging points 1 and 2 are smaller than that of gauging point 3 due to the lateral deflection. During the initial stage, obvious longitudinal stress (σ_v) existed in the tube because the transmission path of friction and bond between concrete and tube was longer, and the hoop stress was nearly zero since the transverse expansion of core concrete was very small. When the applied load attained 75% of ultimate strength, the stresses increased rapidly. At the peak point, only the tube at gauging point 3 yielded, and the hoop stress exhibited a lower level compared to the corresponding longitudinal stress. Compared to short columns, the tube confinement of slender columns cannot be sufficiently utilized.

4. Nonlinear analysis

4.1 Material properties

ABAQUS (v6.12) was used in the analysis of circular TSRC columns. An elastic-plastic model consisting of five stages (see Fig. 11(a)) was used to describe the mechanical behavior of the mild steel with yield strength of 300MPa and 400MPa. More details of this stress-strain relationship can be found in Han *et al.* (2001). The bi-linear model (see Fig. 11(b)) was adopted for the study of the high strength steel with yield strength of 500MPa, and the Young's modulus at the strain-hardening stage was chosen as $0.01E_s$.

The damage plasticity model was used in the analysis of concrete. For TSRC column, the strength and plasticity of core concrete increased since the core concrete is subjected to triaxial loading due to the confinement of the steel tube. In ABAQUS, strength improvement can be achieved by the definition of yielding surface (Lubliner *et al.* 1989). However, the plastic behavior cannot be accurately described by using the stress-strain curves of plain concrete since the strain corresponding to the maximum stress would increase and the descending branch of stress-strain curves tended to become even. A stress-strain model for confined concrete proposed by Mander *et al.* (1988) provided reasonably good prediction for various tests. To simulate the plastic behavior of core concrete, an equivalent stress-strain model was proposed after modification of Mander's model.

Fig. 12 shows the equivalent stress-strain curves for both unconfined (f_l=0MPa) and confined concrete (f_l=0.5MPa), and the equivalent stress-strain relationship is given as follows

$$f = \frac{f_{co} xr}{r - 1 + x^r} \tag{2a}$$

$$x = \varepsilon / \varepsilon_{FE} \tag{2b}$$

$$\varepsilon_{FE} = \varepsilon_{cc} - \left(\frac{f_{cc}}{f_{co}} - 1\right)\varepsilon_{co} \quad (2c)$$

$$\varepsilon_{cc} = \left[1 + 5\left(\frac{f_{cc}}{f_{co}} - 1\right)\right]\varepsilon_{co} \quad (2d)$$

$$\varepsilon_{co} = \left(700 + 172\sqrt{f_{co}}\right) \times 10^{-6} \quad (2e)$$

$$r = \frac{E_c}{E_c - E_{sec}} \quad (2f)$$

$$E_c = 4730\sqrt{f_{co}} \quad (2g)$$

$$E_{sec} = f_{cc} / \varepsilon_{cc} \quad (2h)$$

The compressive strength of confined concrete can be calculated as follows (Mander *et al.* 1988, Li *et al.* 2001)

$$f_{cc} = \begin{cases} f_{co}\left(-1.254 + 2.254\sqrt{1 + 7.94\frac{f_l}{f_{co}}} - 2\frac{f_l}{f_{co}}\right) & f_{co} < 50\text{MPa} \\ f_{co}\left(-0.413 + 1.413\sqrt{1 + 11.4\frac{f_l}{f_{co}}} - 2\frac{f_l}{f_{co}}\right) & f_{co} \geq 50\text{MPa} \end{cases} \quad (3)$$

where f_l is the effective confining stress of the tube that can be calculated using Eq. (4)

$$f_l = 2tf_h / (D - 2t) \quad (4)$$

where f_h is the average hoop stress of the steel tube at yield point for short columns or peak load point for slender columns. Fig. 13 shows the statistical results of the average hoop stress. As can be seen, f_h decreases with an increasing L_t/D ratio, where L_t is the length of the steel tube ($L_t = L$-200mm). If the length-to-diameter ratio is zero, there is no bond and friction between the steel tube and the concrete core, so the hoop stress of the column at failure can reach the yield strength of the steel tube. If the length-to-diameter ratio is infinity, the hoop stress will be negligible since the failure of the column is caused by elastic buckling. According to the analysis above, a regression equation was proposed for the calculation of f_h

$$f_h = \frac{f_{yt}}{0.2 \times (L_t / D)^{1.5} + 1} \quad (5)$$

4.2 Element type and interface

The steel tube and the encased steel section were modeled using 4-node shell elements with reduced integration (S4R). The concrete core was modeled using 8-node brick elements (C3D8R). A surface-based interaction with a contact pressure model in the normal direction and a Coulomb friction model in the tangential direction to the surface between the steel tube and core concrete (Han *et al.* 2007) was used in the FE analysis. The friction coefficient between the two faces was chosen as 0.6. An average surface bond stress (τ_{bond}) of 0.6MPa was used in the Coulomb friction model. As aforementioned, the test results indicated that the studs had no significant influence on the failure mode, strength, and ductility of the specimens, thus the studs were not considered in the FE model. The embedded element technique was used to model the encased steel section.

4.3 Global imperfection and model verification

The global imperfection must be considered when analyzing the stability failure induced by second-order effects. An initial out-of-straightness of *L*/1000 was adopted for calculating the capacity of steel columns in Chinese Standard GB50017 (2003), and an amplitude of *L*/200 was recommended in Eurocode4 (2004) for circular steel tubular columns filled with SRC. The initial eccentricity was chosen as *L*/2000 for the calculations of SRC columns and fibre reinforced concrete-filled stainless steel tubular columns (Ellobody and Young 2011, Ellobody 2013).

The effect of initial imperfections was analyzed using two imperfection amplitudes: *L*/1000 and *L*/200. Fig. 14 shows the imperfection sensitivity of the slender circular TSRC columns. As expected, the ultimate strength and flexural stiffness decrease with the increasing amplitude of the imperfection. The strength of the column with initial eccentricity shows a slight reduction compared to that of the column with the same amplitude of out-of-straightness. The decrease in strength is within 2.2%. Therefore, it is reasonable to take the alternative factor (initial out-of-straightness or initial eccentricity) as the global imperfection of the slender column.

Based on the analysis above, initial eccentricity was adopted as the global imperfection for FE analysis. The global imperfection amplitude of *L*/500, which is approximately equal to the average measured value (the result of specimen C-200-6-S was not taken into account), was found to result in the most accurate agreement according to the tentative calculations. As can be seen from Figs. 5 and 8, good agreement is observed between the predicted results and test results. The model can be used for further parametric analysis.

4.4 Parametric analysis

The influences of steel yield strength (f_{yt} and f_{ys}), concrete strength (f_{co}) and diameter of cross-section (D) are analyzed, as shown in Fig. 15.

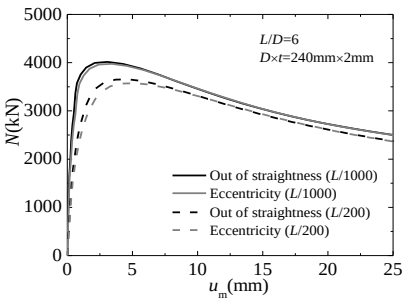

Fig. 14 Imperfection sensitivity of slender columns

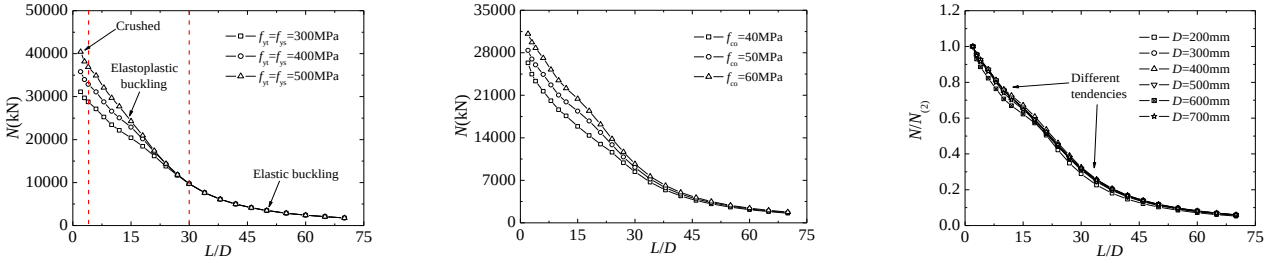

(a) Steel yield strength (b) Concrete strength (c) Diameter of cross-section

Fig. 15 Effects of different parameters on N (or $N/N_{(2)}$) versus L/D ratio curves

The basic calculating conditions of the examples in Fig. 15 are D = 600 mm, f_{yt} = f_{ys} = 300 MPa, and f_{co} = 60 MPa.

Fig. 15(a) shows the N versus L/D ratio curves of columns with different steel yield strengths. Generally, the curves can be divided into three stages. When the L/D ratio is less than or equal to 4, the column fails by steel yielding and concrete crushing. With the increase in the L/D ratio, the failure of the column changes from concrete crushing to elastoplastic buckling. The disparity in the ultimate strengths of the columns with different steel yield strengths decreases with the increasing L/D ratio. When the L/D ratio is greater than 30, the column fails due to elastic buckling. Thus, the columns with different steel strengths exhibit the same capacities. The columns with different f_{co} show a similar tendency, as shown in Fig. 15(b). In the elastic buckling stage, the ultimate strengths of columns with different f_{co} show a slight difference due to the different E_c. Fig. 15(c) shows the size sensitivity of the columns, where $N_{(2)}$ in the figure represents the ultimate strength of the column with L/D = 2. The diameter is observed to have a moderate influence on the relative strength $N/N_{(2)}$. Due to the different failure modes, the curves show two different tendencies.

5. Design method

The components of TSRC columns are more consistent with those of CFST columns. Therefore, the calculating methods for CFST column will be used for reference to predict the ultimate strength of TSRC column under axial compression.

5.1 Eurocode 4

According to Eurocode4, the ultimate strength of composite steel and concrete column under axial compression can be calculated using Eq. (6). The ultimate strengths obtained from the FE results are compared with the unfactored design strengths N_u^{EC4}, as shown in Fig. 16. Although the increase in strength of concrete caused by confinement is taken into consideration in Eurocode4, the predicted results are still conservative due to the underestimation of the tube confinement on the concrete core. At the elastic buckling stage, the predicted results are also conservative due to the underestimation of effective flexural stiffness of the column.

$$N_u^{EC4} = \varphi N_{pl,Rd} \tag{6a}$$

$$\varphi = \frac{1}{\Phi + \sqrt{\Phi^2 - \bar{\lambda}^2}}, \text{ but } \varphi \le 1.0 \tag{6b}$$

$$\Phi = 0.5\left[1 + 0.34\left(\bar{\lambda} - 0.2\right) + \bar{\lambda}^2\right] \tag{6c}$$

5.2 AISC standard

According to AISC, the ultimate strength can be calculated using Eq. (7). The ultimate strengths obtained from the FE results are compared with the unfactored design strengths N_u^{AISC}, as shown in Fig. 17. Similar to the predicted results of Eurocode4, the predicted results of AISC are also conservative when the relative slenderness is small. However, at the elastic buckling stage, the predicted results of AISC show good agreement with the FE results, which indicated that the effective flexural stiffness of TSRC column can be calculated according to AISC.

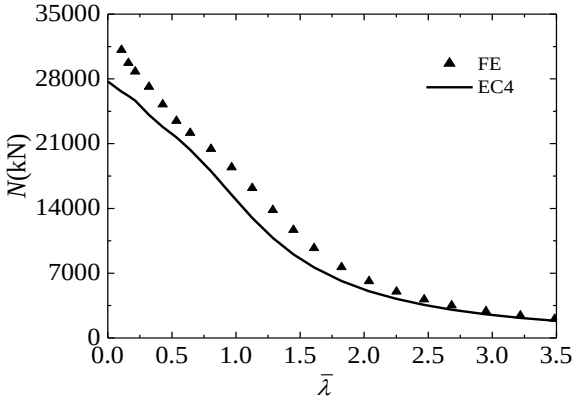

Fig. 16 Comparison between ultimate strengths obtained from FE results and Eurocode4 predictions

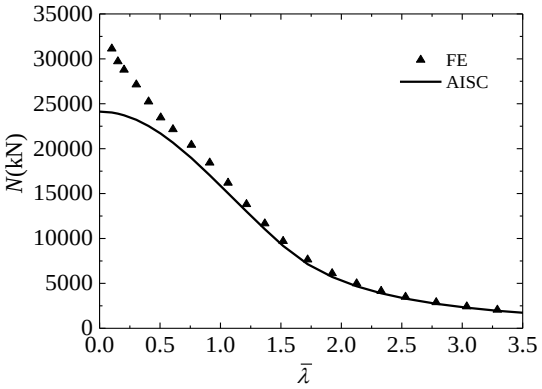

Fig. 17 Comparison between ultimate strengths obtained from FE results and AISC predictions

when $P_e \geq 0.44P_o$

$$N_u^{AISC} = P_o\left[0.658^{\left(\frac{P_o}{P_e}\right)}\right] \tag{7a}$$

when $P_e < 0.44P_o$

$$N_u^{AISC} = 0.877P_e \tag{7b}$$

5.3 Proposed method

The influences of the steel tube on the resistance of TSRC column can be mainly divided into two respects: the direct resistance and the confinement on concrete. As aforementioned, the tube confinement decreases with the increase in slenderness ratio of the column, and the direct resistance is just opposite. These characteristics show distinguishing difference between TSRC column and conventional composite column. Therefore, the strength of circular TSRC cross-section (N_0) is considered to be the sum of three parts, namely the equivalent strength of steel tube, the strength of confined concrete, and the strength of steel section, as shown in Eq. (8).

$$N_0 = A_t f_v + A_c f_{cc} + A_s f_{ys} \tag{8}$$

where A_t, A_c, and A_s are the cross-sectional area of the steel tube, concrete, and steel section, respectively.

The steel tube can be considered as yielding when calculating the ultimate strength of cross-section. According to von Mises yield criterion, the longitudinal stress (f_v) can be calculated as follows

$$f_v = \left(\sqrt{4f_{yt}^2 - 3f_h^2} - f_h\right)/2 \tag{9}$$

When the influence of slenderness ratio is considered, the ultimate strength of circular TSRC column can be calculated using the equation

$$N_u = \varphi N_0 \tag{10}$$

Fig. 18 shows the statistical results of the test and FE simulation. According to the results, the proposed φ can be calculated using Eq. (11). It should be noted that for a given cross-section, the ultimate strengths of the cross-section of the column with different slenderness ratios are different due to the variable tube confinement. This is a key characteristic of TSRC column.

when $\bar{\lambda} \leq 0.285$

$$\varphi = 1 \tag{11a}$$

when $\bar{\lambda} > 0.285$

$$\varphi = \left[1+(1+\varepsilon_0)/\bar{\lambda}^2\right]/2 - \sqrt{\left[1+(1+\varepsilon_0)/\bar{\lambda}^2\right]^2/4 - 1/\bar{\lambda}^2} \tag{11b}$$

where

$$\bar{\lambda} = \sqrt{\frac{N_0}{N_{cr}}} \tag{11c}$$

$$N_{cr} = \frac{\pi^2 (EI)_{eff}}{L_e^2} \tag{11d}$$

$$(EI)_{eff} = E_t I_t + E_s I_s + CE_c I_c \tag{11e}$$

$$C = 0.6 + 2\left(\frac{A_t + A_s}{A_c + A_t + A_s}\right) \leq 0.9 \tag{11f}$$

$$\varepsilon_0 = 0.214\bar{\lambda} - 0.061 \tag{11g}$$

In Eq. (11), φ is the reduction factor; ε_0 is the equivalent imperfection factor; $\bar{\lambda}$ is the non-dimensional slenderness; N_{cr} is the elastic critical force; $(EI)_{eff}$ is the characteristic value of the effective flexural stiffness and C is a correction factor.

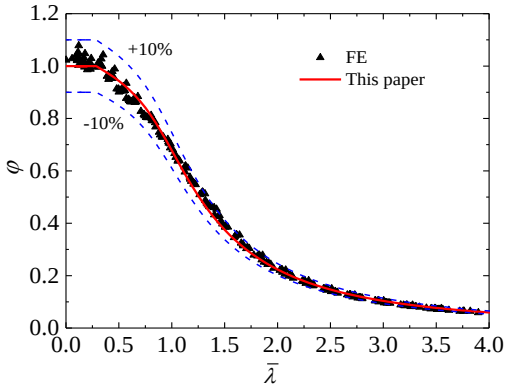

Fig. 18 Comparison of predictions obtained from proposed method with FE results

Table 2 Comparisons of test results and calculated results

Specimen	L_e (mm)	N_{ue} (kN)	Eurocode4				AISC				Proposed method			
			$\bar{\lambda}$	φ	N_u^{EC4}	N_u^{EC4}/N_{ue}	$\bar{\lambda}$	φ	N_u^{AISC}	N_u^{AISC}/N_{ue}	$\bar{\lambda}$	φ	N_u	N_u/N_{ue}
C-200-3	445	3421	0.127	1	2841	0.830	0.122	0.989	2591	0.757	0.126	1	3067	0.896
C-200-3-S	445	3423	0.127	1	2841	0.830	0.122	0.989	2591	0.757	0.126	1	3067	0.896
C-200-6	1300	2851	0.370	0.938	2535	0.889	0.355	0.949	2473	0.867	0.356	0.983	2829	0.992
C-200-6-S	1300	2933	0.370	0.938	2535	0.864	0.355	0.949	2473	0.843	0.356	0.983	2829	0.965
C-240-3	505	4408	0.121	1	3893	0.883	0.115	0.989	3521	0.799	0.122	1	4227	0.959
C-240-3-S	505	4400	0.121	1	3893	0.885	0.115	0.989	3521	0.800	0.122	1	4227	0.961
C-240-6	1540	3797	0.369	0.938	3456	0.910	0.352	0.949	3362	0.885	0.358	0.982	3875	1.021
C-240-6-S	1540	3439	0.369	0.938	3456	1.005	0.352	0.949	3362	0.978	0.358	0.982	3875	1.127
					Mean	0.887			Mean	0.836			Mean	0.977
					COV	0.062			COV	0.089			COV	0.076

* L_e: For short column, L_e=(L+290)/2; for slender column, L_e=L+100, see Fig. 3

The ultimate strengths of all the specimens are calculated using Eurocode4, AISC, and the proposed method. Table 2 lists the comparisons of the test results and the predicted results, where L_e is the effective length of the column. As observed, the predicted results of Eurocode4 and AISC are conservative due to the underestimation of the confinement on concrete core. The average value of N_u^{EC4}/N_{ue} is 0.881 with the corresponding COV of 0.067, and the average value of N_u^{AISC}/N_{ue} is 0.834 with the corresponding COV of 0.091. From the comparison, the predicted strengths using the proposed method show good agreement with the test data. As a result, the average value of N_u/N_{ue} is 0.973 with the corresponding COV of 0.079.

6. Conclusions

This paper presented experimental investigation and nonlinear analysis on the axial load behavior of circular TSRC columns. Eight columns were tested to investigate the effect of length-to-diameter ratio (L/D) of the specimens, diameter-to-thickness ratio (D/t) of the steel tubes, and use of stud shear connectors on the steel sections. The design philosophy for circular TSRC columns was discussed, and the following conclusions were drawn from the study:

- With the increase in the L/D ratio, the failure of the circular TSRC column changes from concrete crushing to elastoplastic buckling. Stud shear connectors are found to have no significant influence on the load-bearing capacity and the elastic stiffness of the specimens.
- The steel tubes yielded when the applied compression almost reached the ultimate value for short columns. Compared to the short columns, the tube confinement of the slender columns cannot be sufficiently utilized.
- A nonlinear FE model was established using ABAQUS. An initial global imperfection with a magnitude of L/500 was recommended in the analysis. The analysis results showed good agreement with the test results.
- The design methods specified in current Eurocode 4 and the AISC standard were used to predict the ultimate strength of the innovative composite columns. The comparisons indicated that the predictions of Eurocode4 and the AISC standard were conservative due to the underestimation of the tube confinement.
- A method for calculating the ultimate strength of this innovative composite column was proposed, and the calculated results agree well with the experimental results.

Acknowledgments

The research work reported herein was made possible by the National Natural Science Foundations of China (no.51308051, no.51622802). The financial supports are highly appreciated.

References

ABAQUS (version 6.12), Dassault Systèmes SIMULIA, Providence, RI.

ACI 318 (2014), Building code requirements for structural concrete and commentary, American Concrete Institute; Farmington Hills, MI, USA.

AISC 360 (2016), Specification for structural steel buildings, American Institute of Steel Construction; Chicago, Illinois,

USA.
Chang, X., Wei, Y.Y. and Yun, Y.C. (2012), "Analysis of steel-reinforced concrete-filled-steel tubular (SRCFST) columns under cyclic loading", *Constr. Bulid. Mater.*, **28**, 88-95.
Chen, Z., Xu, J., Chen, Y. and Xue, J. (2016), "Axial compression ratio limit values for steel reinforced concrete (SRC) special shaped columns", *Steel Compos. Struct.*, **20**(2), 295-316.
Choi, E.G., Kim, H.S. and Shin, Y.S. (2012), "Performance of fire damaged steel reinforced high strength concrete (SRHSC) columns", *Steel Compos. Struct.*, **13**(6), 521-537.
El-Tawil, S. and Deierlein, G.G. (1999), "Strength and ductility of concrete encased composite columns", *J. Struct. Eng.*, **125**(9), 1009-1019.
Ellobody, E. (2013), "Numerical modelling of fibre reinforced concrete-filled stainless steel tubular columns", *Thin Wall. Struc.*, **63**, 1-12.
Ellobody, E. and Young, B. (2011), "Numerical simulation of concrete encased steel composite columns", *J. Constr. Steel. Res.*, **67**(2), 211-222.
Eurocode 4 (2004), Design of composite steel and concrete structures. Part 1.1: General rules and rules for buildings, European Committee for Standardization; Brussels, Belgium.
Gan, D., Guo, L.H., Liu, J.P. and Zhou, X.H. (2011), "Seismic behavior and moment strength of tubed steel reinforced-concrete (SRC) beam-columns", *J. Constr. Steel. Res.*, **67**(10), 1516-1524.
Gardner, N.J. and Jacobson, E.R. (1967), "Structural behavior of concrete filled steel tubes", *ACI J. Proc.*, **64**(7), 404-413.
GB50017 (2003), Code for design of steel structures, Ministry of Housing and Urban-Rural Development of China; Beijing, China. (in Chinese)
Han, L.H., Yao, G.H. and Tao, Z. (2007), "Performance of concrete-filled thin-walled steel tubes under pure torsion", *Thin Wall. Struct.*, **45**(1), 24-36.
Han, L.H., Zhao, X.L. and Tao, Z. (2001), "Tests and mechanics model for concrete-filled SHS stub columns, columns and beam-columns", *Steel Compos. Struct.*, **1**(1), 51-74.
Ky, V.S., Tangaramvong, S. and Thepchatri, T. (2015), "Inelastic analysis for the post-collapse behavior of concrete encased steel composite columns under axial compression", *Steel Compos. Struct.*, **19**(5), 1237-1258.
Liu, J.P., Wang, X.D., Qi, H.T., et al. (2015), "Behavior and Strength of Circular Tubed Steel-Reinforced-Concrete Short Columns under Eccentric Loading", *Adv. Struct. Eng.*, **18**(10), 1587-1595.
Lubliner, J., Oliver, J., Oller, S. and Oñate, E. (1989), "A plastic-damage model for concrete", *Int. J. Solids Struct.*, **25**(3), 299-326.
Massone, L.M., Sayre, B.L. and Wallace, J.W. (2017), "Load-Deformation responses of slender structural steel reinforced concrete walls", *Eng. Struct.*, **140**, 77-88.
Tomii, M., Sakino, K., Xiao, Y. and Watanabe, K. (1985), "Earthquake resisting hysteretic behavior of reinforced concrete short columns confined by steel tube", *Proceedings of the International Speciality Conference on Concrete Filled Steel Tubular Structures*, Harbin, China, August.
Wang, Q.W., Shi, Q.X. and Tian H.H. (2015), "Seismic behavior of steel reinforced concrete (SRC) joints with new-type section steel under cyclic loading", *Steel Compos. Struct.*, **19**(6) , 1561-1580.
Wang, X.D., Liu, J.P. and Zhou, X.H. (2016), "Behaviour and design method of short square tubed-steel-reinforced-concrete columns under eccentric loading", *J. Constr. Steel. Res.*, **116**, 193-203.
Zhou, X.H. and Liu, J.P. (2010), *Performance and Design of Steel Tube Confined Concrete*. Science Press, Beijing, China. (in Chinese)

BU